

# ReLoc: A Restoration-Assisted Framework for Robust Image Tampering Localization

Peiyu Zhuang, Haodong Li, Rui Yang, Jiwu Huang,

**Abstract**—With the spread of tampered images, locating the tampered regions in digital images has drawn increasing attention. The existing image tampering localization methods, however, suffer from severe performance degradation when the tampered images are subjected to some post-processing, as the tampering traces would be distorted by the post-processing operations. The poor robustness against post-processing has become a bottleneck for the practical applications of image tampering localization techniques. In order to address this issue, this paper proposes a novel *restoration-assisted* framework for image tampering localization (ReLoc). The ReLoc framework mainly consists of an image restoration module and a tampering localization module. The key idea of ReLoc is to use the restoration module to recover a high-quality counterpart of the distorted tampered image, such that the distorted tampering traces can be re-enhanced, facilitating the tampering localization module to identify the tampered regions. To achieve this, the restoration module is optimized not only with the conventional constraints on image visual quality, but also with a forensics-oriented objective function. Furthermore, the restoration module and the localization module are trained alternately, which can stabilize the training process and is beneficial for improving the performance. The proposed framework is evaluated by fighting against JPEG compression, the most commonly used post-processing. Extensive experimental results show that ReLoc can significantly improve the robustness against JPEG compression. The restoration module in a well-trained ReLoc model is transferable. Namely, it is still effective when being directly deployed with another tampering localization module.

**Index Terms**—Image forensics, tampering localization, image restoration, robustness against post-processing

## I. INTRODUCTION

AS an important carrier of information transmission, digital images appear widely in our daily life. With the development of image processing technology, people can easily create realistic tampered images by using various image editing software. Once the tampered images are used for malicious purposes, such as forging certificates, creating rumors, *etc.*, it is bound to result in a series of negative impacts. Therefore, in order to prevent the abuse of tampered images, it is of great significance to identify tampered images.

In recent years, many forensic methods have been proposed to detect tampered images and further localize the tampered

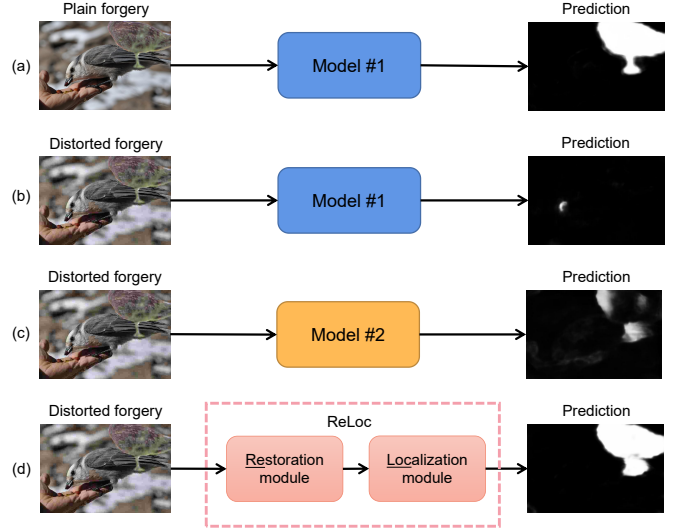


Fig. 1. Tampering localization results in different situations. The localization model #1 was trained with plain tampered images, model #2 was fine-tuned with distorted images based on model #1, and the localization module in ReLoc was fine-tuned with restored images.

regions [1], [2]. The technological paradigms of these methods have shown a trend from relying on hand-crafted features [3]–[5] to utilizing deep learning techniques [6]–[18]. Nowadays, the deep learning (DL)-based forensic methods usually achieve much better performance than the conventional ones. For one thing, this can be attributed to the use of some effective network architectures, such as fully convolutional network [19], U-Net [20], faster R-CNN [21], mask-RCNN [22] and ViT [23]. For another thing, the combination of deep learning and domain knowledge in forensics also plays an important role [24], [25].

Although the existing tampering localization methods can achieve good performance on some datasets in laboratorial evaluations, in practical applications they suffer from severe performance degradation when the tampered images are subjected to a series of post-processing operations, such as JPEG compression, blurring, scaling, *etc.* Because post-processing would seriously distort the tampering traces. For conciseness, hereinafter we refer the tampered images without post-processing as *plain images* and the post-processed counterparts as *distorted images*. The phenomenon mentioned above can be intuitively interpreted with Fig. 1. Generally, a tampering localization model is trained with a set of plain images. The model works well if the investigated image is a plain forgery (Fig. 1-a). However, if a distorted tampered image

Corresponding author: Haodong Li.

P. Zhuang, H. Li, and J. Huang are with the Guangdong Key Laboratory of Intelligent Information Processing and Shenzhen Key Laboratory of Media Security, Shenzhen University, Shenzhen 518060, China; and also with the Shenzhen Institute of Artificial Intelligence and Robotics for Society, Shenzhen 518060, China. (email: 1800261051@email.szu.edu.cn; lihaodong, jwhuang@szu.edu.cn)

R. Yang is with the Alibaba Group, Hanzhou 311121, China. (email: duming.yr@alibaba-inc.com)

is fed to the model, the tampered regions are likely failed to be identified (Fig. 1-b). As a result, post-processing has become a stumbling stone for the practical applications of image tampering localization.

In order to improve the robustness against post-processing, some recent works have tried to introduce distorted images in the training phase. Rao *et al.* [26] proposed to learn robust features from JPEG proxy images. They employed a JPEG proxy network to simulate the process of JPEG compression and produce JPEG proxy images. The proxy images were then used to train the localization model. To obtain a robust model against online social networks (OSN), Wu *et al.* [10] firstly simulated the noise introduced by OSN and then introduce the noise into the training images to generate distorted images. However, since the tampering traces have been distorted by post-processing, it is difficult to learn discriminative features. As shown in Fig. 1-c, even though the localization network was fine-tuned directly with distorted images, the tampered regions cannot be well detected.

Different from the existing approaches, this paper tries to improve the robustness against post-processing from a novel perspective. Our key idea is that, once the tampering traces distorted by post-processing can be recovered or re-enhanced, it is able to learn effective representations for tampering localization. To this end, we propose a *restoration-assisted* framework for robust image tampering localization (ReLoc). ReLoc is a hybrid framework that cascades a restoration module and a localization module (Fig. 1-d). The restoration module aims to re-enhancing the distorted tampering traces and recovering a high-quality counterpart from the distorted image. The localization module takes the restored images as input, so that the subtle tampering traces would be captured more efficiently. We utilize a pixel-level loss, an image-level loss, and a forensics-oriented localization loss to train the restoration module. In this way, the restoration module is jointly constrained by image visual quality and tampering localization efficacy. We also propose to optimize the restoration and localization modules in an alternate way, which can make the training process more stable and achieve better performance. To evaluate the effectiveness of ReLoc, we consider a typical case on handling against JPEG compression, which is one of the most commonly used post-processing operations. The extensive experiments involving three tampering localization methods on three different datasets show that ReLoc can significantly improve the robustness against JPEG compression, regardless of whether the compression quality is fixed or changeable. Another merit of ReLoc is that the restoration module in a well-trained model is transferable, meaning that it can be directly deployed with another localization module for improving the robustness of tampering localization.

The main contributions of this work are as follows.

- We propose a new idea to improve the robustness of tampering localization against post-processing. That is, to restore the distorted image before performing tampering localization. Based on this idea, we propose a restoration-assisted tampering localization framework (ReLoc). By utilizing the restoration module, the distorted tampering

traces can be recovered to some extent, so that the tampering localization module can capture tampering traces more efficiently. Consequently, the robustness will be improved. To our best knowledge, this is the first work to utilize image restoration to achieve robust tampering localization.

- We design a training schema for ReLoc that is tailored for image tampering localization. To train the restoration module, in addition to considering image visual quality, we also include a forensics-oriented loss for ensuring tampering localization performance. To make the training process stable, we optimize the restoration and localization modules in an alternate way. The experimental results show that the proposed method can effectively improve the robustness against post-processing.
- We provide a plug-and-play restoration module for robust tampering localization via introducing the ReLoc framework. We experimentally validate that the restoration module in a well-trained ReLoc model is also effective to work with another localization module, meaning that ReLoc can be flexibly deployed in practical applications.

The rest of this paper is organized as follows. Section II reviews the related works on image restoration and image tampering localization. Section III describes the proposed framework in detail. Section IV presents the experimental results and discussions. Finally, Section V draws the concluding remarks.

## II. RELATED WORK

### A. Image Restoration

As a fundamental problem in image processing, image restoration aims to recover visually pleasant high-quality images from degraded low-quality images. Usually, the degraded images are subjected to different distorted operations, such as down-sampling, blurring, and lossy compression. As a result, image restoration includes denoising, super-resolution, deblurring, *etc.* Image restoration is an ill-posed inverse problem. To solve such a problem, conventional methods usually resort to certain image priors and mathematical models [27]–[29]. Recently, the research of image restoration has been dominated by DL-based methods, as deep learning is very effective for improving image visual quality.

The DL-based image restoration methods usually employ convolutional neural network (CNN) [30] or Transformer [31] as basic architectures. Dong *et al.* [32] proposed the first CNN-based image super-resolution method, in which the model was constructed by stacking convolutional layers. They also applied CNN to the reduction of JPEG compression artifacts [33]. By adopting residual learning, Kim *et al.* [34] proposed a method for image super-resolution. In order to make use of the hierarchical features extracted at different levels in CNNs, Zhang *et al.* [35] proposed a residual dense network for image super-resolution, denoising, and deblurring. Recently, with the promising performance achieved by Vision Transformer [23], Transformer-based methods have become popular in the field of image restoration, such as U-Former [36] and SwinConv-Unet [37].

In addition to network architectures, the objective functions also play an important role in image restoration. While pixel-level MAE and MSE losses are commonly used for optimization, they tend to produce smooth images. To alleviate this issue, the perceptual loss [38] is used to make the restoration images more pleasant for human eyes.

Since image restoration can recover the information loss caused by degradation to a certain extent, it is beneficial for some high-level vision applications, such as image classification, semantic segmentation, and object detection, in the case that the given images are distorted ones. Haris *et al.* [39] proposed to optimize a super-resolution network for object detection in low-resolution images. To improve the performance of semantic segmentation for distorted images, Niu *et al.* [40] applied denoising and super-resolution to the input images through a restoration network. In this paper, we build a bridge between image restoration and image forensics. To our best knowledge, this is the first work to show that incorporating an image restoration module with a tampering localization module can significantly improve the tampering localization performance for distorted images.

### B. Image Tampering Localization

Image tampering detection and localization methods are in urgent need as the increasing abuse of tampered images in our daily life. With the development of deep learning, many DL-based tampering detection and localization methods have been proposed [2]. Some of them are targeted for a certain tampering operation, such as splicing [6], [7], copy-move [41], and inpainting [11], [12]. On the other hand, some are designed for general detection. Wu *et al.* [14] trained a feature extractor with 385 types of tampering operations, and then built a local anomaly detection network based on LSTM to predict the tampered regions. Liu *et al.* [15] proposed a PSCC-Net, which made use of the attention mechanism [42] and performed tampering localization at different scales through a progressive network structure. Chen *et al.* [43] proposed a MVSS-net for tampering localization by leveraging the multi-view and multi-scale information. To capture the subtle tampering traces, Zhuang *et al.* [16] designed a network with the dense block [44] and included the commonly used operations in Photoshop to build a dataset for pre-training. Kwon *et al.* [45] performed tampering localization with dual-domain information. They used a DCT branch to capture JPEG compression traces and fused the features extracted from a spatial branch. As Transformer [31] can better model the global information, some tampering localization methods based on Transformer have also been developed, such as TransForensics [17] and ObjectFormer [18]. Despite the above methods can obtain good performance on some datasets, they did not address the robustness against post-processing through an explicitly algorithmic design. As a result, their performance would be significantly degraded in practical situations.

To improve the robustness against post-processing, some efforts have been conducted. For example, Abecidan *et al.* [46] improved the robustness to JPEG compression by using domain adaptation between the source and target domains,

so that the detector was constrained to learn a robust feature representation. Rao *et al.* [26] simulated the impact of JPEG compression by generating proxy images, which can facilitate the learning of tampering traces when the images are undergone JPEG compression. Wu *et al.* [10] considered handling the tampering images that are transmitted through online social networks. They firstly estimated the noise introduced by OSN transmission. Then, they augmented the tampered images with the predicted noise and trained the detector to make it robust to online transmission. Although these works explicitly consider post-processing operations, the detectors are difficult to learn effective features from the distorted images, due to the fact that the tampering traces have been weakened by post-processing. Different from them, we design a new framework to address the problem of robustness. In the proposed method, a given distorted image is processed by a restoration module before being fed to a tampering localization module. In this way, the tampering traces can be recovered to some extent, promoting the localization module to learn more robust features.

## III. PROPOSED METHOD

In this section, we elaborate on the proposed restoration-assisted framework for robust image tampering localization (ReLoc). We first analyze the feature representation under different situations, so as to give a better understanding of the intrinsic mechanism of the robustness problem. After that we give an overview of ReLoc, and then describe how to design a forensics-oriented restoration task and how to optimize the overall framework.

To make the descriptions concise in the following contexts, we denote a plain image, a distorted image, and a restored image as  $\mathbf{I}^P$ ,  $\mathbf{I}^D$ , and  $\mathbf{I}^R$ , respectively. We also denote a model as  $\mathcal{M}$  and use a superscript to indicate its training situation. Namely,  $\mathcal{M}^P$  and  $\mathcal{M}^{D|P}$  mean a model trained with a set of  $\mathbf{I}^P$  and a model further fine-tuned with a set of  $\mathbf{I}^D$ , respectively. For a model built with ReLoc, it is denoted as  $\mathcal{M}^{ReLoc}$ , and the restoration module and localization module are denoted as  $\mathcal{M}_R^{ReLoc}$  and  $\mathcal{M}_L^{ReLoc}$ , respectively. To describe a testing situation that a set of image  $\mathbf{I}^*$  is fed to a trained model  $\mathcal{M}^*$ , we refer to  $\mathcal{M}^*\{\mathbf{I}^*\}$ . In this way, the four situations shown in Fig. 1 are denoted as  $\mathcal{M}^P\{\mathbf{I}^P\}$ ,  $\mathcal{M}^P\{\mathbf{I}^D\}$ ,  $\mathcal{M}^{D|P}\{\mathbf{I}^D\}$ , and  $\mathcal{M}^{ReLoc}\{\mathbf{I}^D\}$ , respectively.

### A. Analysis of Feature Representations

In order to improve the robustness against post-processing, a straightforward approach is to introduce the corresponding post-processing operations in the training phase. Namely, to train a model with distorted images and expect that it can learn robust feature representation. However, as the tampering traces in the distorted images have been weakened by post-processing, it is tricky for the tampering localization model to learn effective features directly from distorted images.

To better interpret what is mentioned above, we analyze the feature representations between tampered pixels and original pixels in different situations. Firstly, we trained tampering localization models based on the network architecture proposed

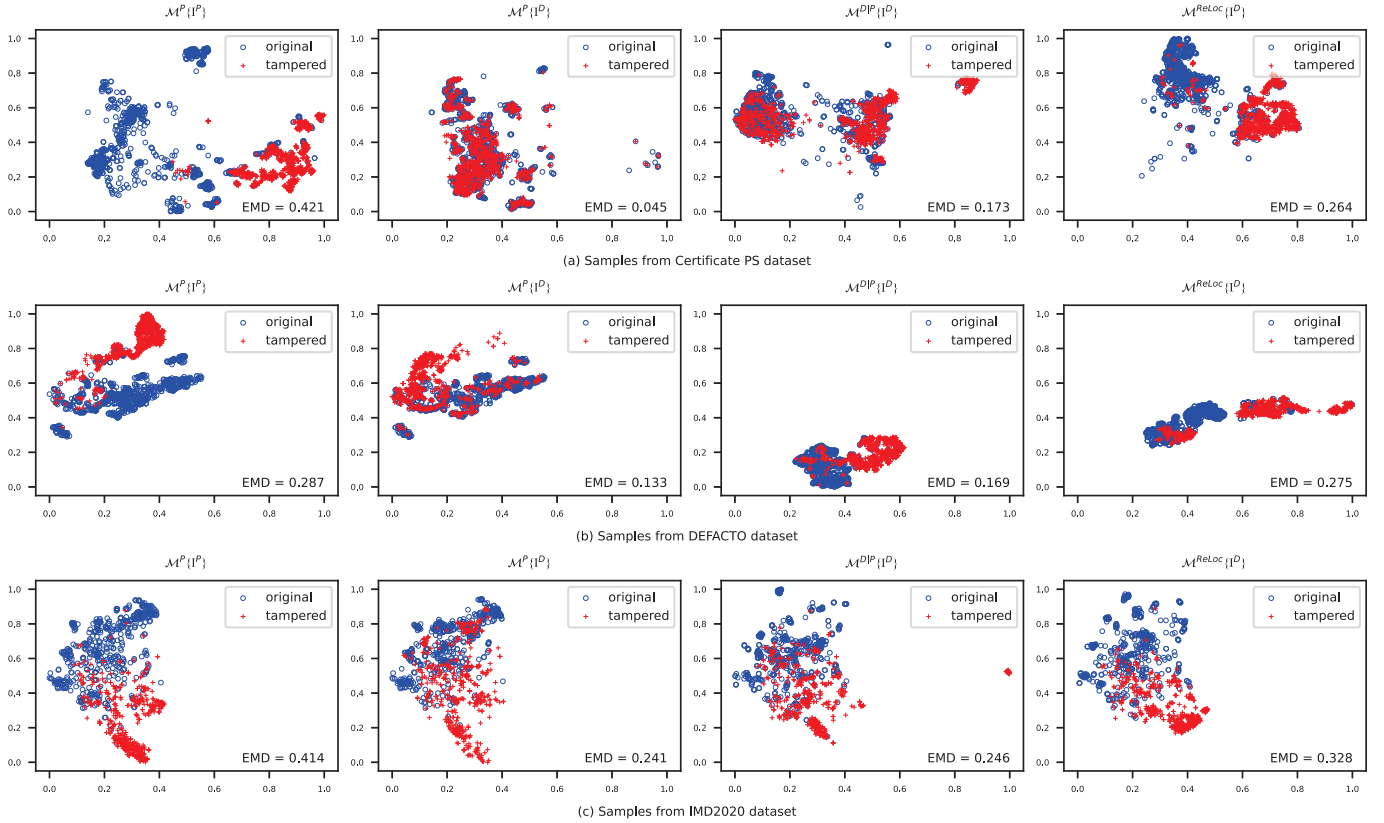


Fig. 2. The feature representations of 1,000 original pixels and 1,000 tampered pixels projected by T-SNE in different situations. The earth mover’s distance (EMD) is used to measure the distance between the distributions of the two types of pixels.

in [10]<sup>1</sup>. By using the trained models, we then tested the tampered images in the Certificate PS dataset (self-created, refer to Section IV-A1 for details), DEFACTO dataset [47], and IMD2020 dataset [48], respectively. We randomly selected 1000 original and 1000 tampered pixels from the tampered images in each dataset and used T-SNE [49] to project their feature representations extracted by the encoder of the trained models to a 2-D space. The scatter plots of the 2-D representations are shown in Fig. 2. As shown in the leftmost column of Fig. 2, in the case  $\mathcal{M}^P\{\mathbf{I}^P\}$  (*i.e.*, a model trained with plain images is used to test plain images), the distribution gaps between the representations of tampered pixels and original pixels are large. At this time, the model can well localize the tampered regions. However, when the tampered images are subjected to lossy post-processing, the tampering traces would be distorted. As shown in the second column of Fig. 2, the distributions of original pixels and tampered pixels become confused, and the distances between the distributions of the two types of pixels are significantly reduced. In this case, the performance of the localization model will be very poor, as shown in Fig. 1-b.

In order to improve the tampering localization performance for distorted images, we can fine-tune the model  $\mathcal{M}^P$  with distorted images and obtain a fine-tuned model  $\mathcal{M}^{D|P}$ , and then test  $\mathbf{I}^D$  with  $\mathcal{M}^{D|P}$ . In this case, as shown in the third

column of Fig. 2, the distances between the distributions of original pixels and tampered pixels increase compared to the case  $\mathcal{M}^P\{\mathbf{I}^D\}$ . However, it is observed that the two distributions are still not as distinguishable as that in the case  $\mathcal{M}^P\{\mathbf{I}^P\}$ . Based on these observations, we conclude that it is difficult to improve the robustness of tampering localization methods by simply training on distorted images. A possible reason is that the post-processing operations have inevitably led to information loss on the tampering traces, and the localization model is difficult to learn effective feature representations for the tampering traces from distorted images due to information loss. To alleviate this issue, there is a need to recover the information loss caused by post-processing.

### B. Overview of ReLoc

Based on the above analysis, we are aware of that the information loss introduced by post-processing increases the difficulty for distinguishing the tampered pixels from the original pixels. Consequently, we propose a new idea to improve the robustness against post-processing. Namely, restoring the distorted images first and then performing tampering localization on the restored images. It is expected that the information loss would be remedied via restoration, so that the tampering localization performance can be further improved. Based on this idea, we propose a restoration-assisted image tampering localization framework, named ReLoc. As shown in Fig. 3, ReLoc mainly consists of a restoration module, a

<sup>1</sup>Similar results can be obtained by using other tampering localization methods, such as [16], [43].

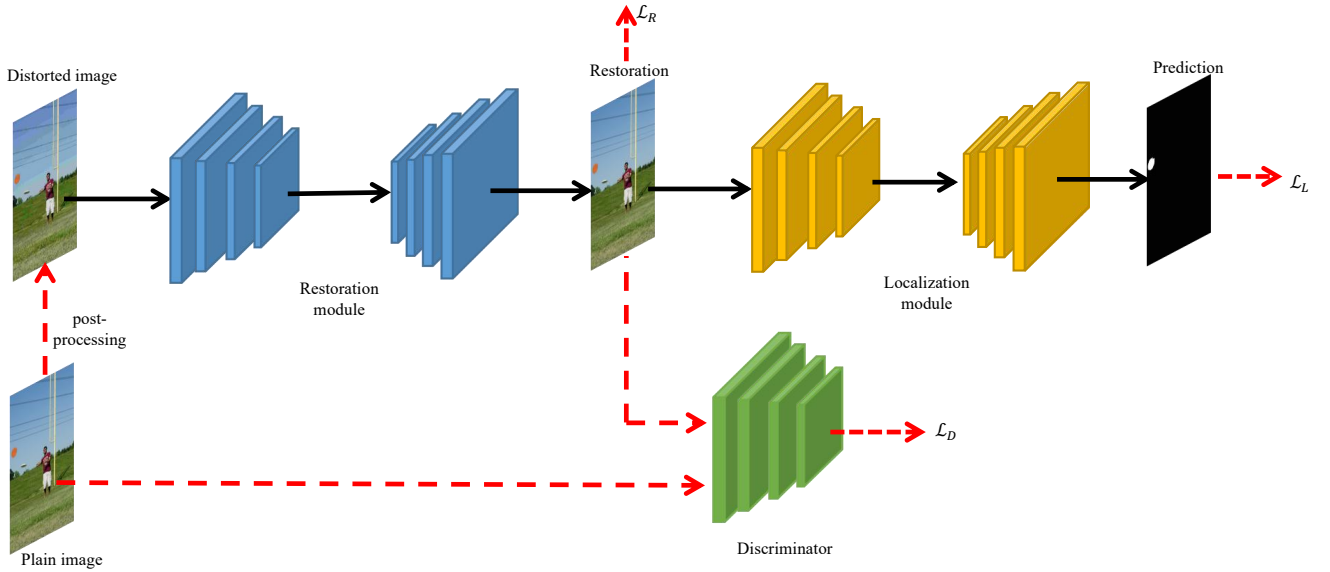


Fig. 3. The diagram of the proposed ReLoc framework. Note that the process represented by the red dotted lines are only applicable for the training process. The restoration and localization modules are shown with encoder-decoder structures in this figure, but they are not limited to such a specific type of structure.

localization module, and a discriminator. For a given distorted image, the restoration module takes it as input and produces a restored image. Then, the tampering localization module infers the tampered regions by using the restored image. The discriminator, aiming to help the restoration module generate better restored images, is utilized only in the training phase. To make the restoration effective, we design different loss functions to optimize the restoration network, including the pixel-level and image-level losses, as well as a loss regarding to forensic performance (Section III-C). To make the whole framework be trained in a stable way, we develop an alternate training strategy for the restoration module and the localization module (Section III-D). As shown in the rightmost column of Fig. 2, by using ReLoc, the distances between the distributions of original pixels and tampered pixels become larger than the cases of  $\mathcal{M}^{D|P}\{\mathbf{I}^D\}$  and  $\mathcal{M}^P\{\mathbf{I}^D\}$ , implying that ReLoc can effectively improve the robustness of tampering localization against post-processing.

### C. Forensics-oriented Restoration

As we know, the degradation process is irreversible and image restoration is an ill-posed inverse problem, meaning that it is unable to completely transform a distorted image to its plain version via restoration. To restore a low-quality image to a visually pleasant high-quality image, existing image restoration methods utilize MAE, MSE, or other perceptual losses to optimize a restoration model. Such losses consider only the visual quality. However, the focuses of human eyes and machines are different [50], [51]. If an image is restored by optimizing only visual quality, the restored image may not be suitable for the task of tampering localization. Therefore, it needs to make a restored image as close as possible to its plain version in several aspects at the same time. To this end, we introduce three different losses to optimize the restoration module, including a pixel-level loss, an image-level loss, and a

forensics-oriented loss. The used losses are described in detail as follows.

1) *Pixel-level loss*: As did in traditional restoration methods, we use a pixel-level MAE loss to measure the distance between every single pixel in a restored image and the corresponding plain image. The pixel-level MAE loss  $\mathcal{L}_{MAE}$  is given as

$$\mathcal{L}_{MAE} = \frac{1}{mn} \sum_{i=1}^m \sum_{j=1}^n |\mathbf{I}_{i,j}^P - \mathbf{I}_{i,j}^R|, \quad (1)$$

where  $\mathbf{I}^P$  denotes the plain tampered image,  $\mathbf{I}^R$  denotes the restored image output from the restoration module, and  $m$  and  $n$  denote the height and width of an image, respectively.

2) *Image-level loss*: The  $\mathcal{L}_{MAE}$  mentioned above focuses on the restoration of each individual pixel, but does not consider the overall statistical distribution of an image. Inspired by adversarial training in the field of image generation, we use an adversarial training strategy to make the restored image as close as possible to the plain tampered image at the image level. We treat the restoration module as a generator and use a discriminator to classify the restored image and the plain image. The discriminator in DCGAN [52] is adopted here. The generative and discriminative losses are formulated as

$$\mathcal{L}_G = -\log f(\mathbf{I}^R; \theta_D), \quad (2)$$

$$\mathcal{L}_D = -\log f(\mathbf{I}^P; \theta_D) - \log(1 - f(\mathbf{I}^R; \theta_D)), \quad (3)$$

where  $\theta_D$  denotes the parameters of the discriminator,  $f(\mathbf{I}^R; \theta_D)$  and  $f(\mathbf{I}^P; \theta_D)$  represent the probabilities output from the discriminator when the inputs are  $\mathbf{I}^R$  and  $\mathbf{I}^P$ , respectively.

3) *Forensics-oriented loss*: Since the purpose of restoration in ReLoc is to make the tampering localization module work better, we should ensure that the distributions of the tampered and original pixels in the restored image are distinct enough,

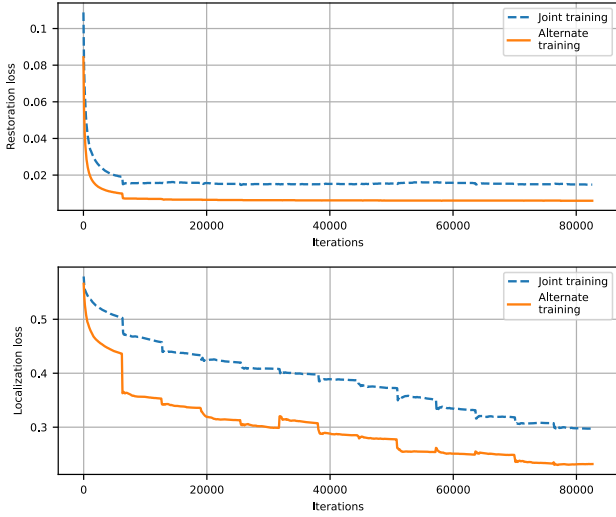


Fig. 4. The training restoration and localization losses for joint training and alternate training.

so that the tampering localization module can distinguish them from each other after restoration. To this end, the localization loss for training the localization module is also used to optimize the restoration module. Specifically, the localization loss is composed of the cross-entropy loss and the dice loss, which are defined as

$$\mathcal{L}_{CE} = -\frac{1}{mn} \sum_{i=1}^m \sum_{j=1}^n [\mathbf{G}_{i,j} \log(\mathbf{P}_{i,j}) + (1 - \mathbf{G}_{i,j}) \log(1 - \mathbf{P}_{i,j})], \quad (4)$$

$$\mathcal{L}_{DICE} = 1 - \frac{2 \sum_{i=1}^m \sum_{j=1}^n \mathbf{P}_{i,j} * \mathbf{G}_{i,j}}{\sum_{i=1}^m \sum_{j=1}^n \mathbf{P}_{i,j}^2 + \sum_{i=1}^m \sum_{j=1}^n \mathbf{G}_{i,j}^2 + \epsilon}, \quad (5)$$

where  $\mathbf{G}$  is the ground-truth map,  $\mathbf{P}$  is the predicted probability map output by the localization module, and  $\epsilon$  is a small constant to avoid zero division. The total localization loss is a weighted sum of  $\mathcal{L}_{CE}$  and  $\mathcal{L}_{DICE}$ :

$$\mathcal{L}_L = \lambda_1 \mathcal{L}_{CE} + (1 - \lambda_1) \mathcal{L}_{DICE}, \quad (6)$$

where  $\lambda_1$  represents the weighting parameter.

On the whole, we incorporate  $\mathcal{L}_L$  with  $\mathcal{L}_{MAE}$  and  $\mathcal{L}_G$  to optimize the restoration module. The total restoration loss is given by

$$\mathcal{L}_R = \lambda_2 \mathcal{L}_{MAE} + \lambda_3 \mathcal{L}_G + \lambda_4 \mathcal{L}_L, \quad (7)$$

where  $\lambda_2$ ,  $\lambda_3$ , and  $\lambda_4$  are the weights for  $\mathcal{L}_{MAE}$ ,  $\mathcal{L}_G$  and  $\mathcal{L}_L$ , respectively.

#### D. Optimization Strategy

As the functions of the restoration module and the localization module in ReLoc are different, an appropriate optimization strategy is important for training the whole framework. Ideally, we can improve the training efficiency of the whole framework by initializing  $\mathcal{M}_L^{ReLoc}$  with the parameters of  $\mathcal{M}^P$  and only training  $\mathcal{M}_R^{ReLoc}$ . However, since image restoration is ill-posed, we cannot perfectly restore the distorted tampered

#### Algorithm 1 The Optimization Algorithm

**Input:**  $\mathbb{D}$ : training dataset;  
 $t$ : total training epochs;  
 $\ell_R$ : learning rate of restoration module;  
 $\ell_D$ : learning rate of discriminator;  
 $\ell_L$ : learning rate of localization module.

**Output:**  $\theta_R$ : trained restoration module;  
 $\theta_L$ : trained localization module.

- 1: Randomly initialize  $\theta_R$  and  $\theta_D$ , and initialize  $\theta_L$  with the weights in  $\mathcal{M}^P$ .
- 2: **for**  $epoch = 1, 2, \dots, t$  **do**
- 3:   **if**  $epoch \bmod 2 \neq 0$  **then**
- 4:     **for** minibatch  $(x_i^P, x_i^D, y_i) \subset \mathbb{D}$  **do**
- 5:        $g_{\theta_D} \leftarrow \nabla_{\theta_D} \mathcal{L}_D$
- 6:        $\theta_D \leftarrow \theta_D - \ell_D \cdot g_{\theta_D}$
- 7:        $g_{\theta_R} \leftarrow \nabla_{\theta_R} \mathcal{L}_R$
- 8:        $\theta_R \leftarrow \theta_R - \ell_R \cdot g_{\theta_R}$
- 9:     **end for**
- 10:    **else**
- 11:     **for** minibatch  $(x_i^P, x_i^D, y_i) \subset \mathbb{D}$  **do**
- 12:        $g_{\theta_L} \leftarrow \nabla_{\theta_L} \mathcal{L}_L$
- 13:        $\theta_L \leftarrow \theta_L - \ell_L \cdot g_{\theta_L}$
- 14:     **end for**
- 15:    **end if**
- 16: **end for**

images to plain images. Therefore, this training strategy would lead to sub-optimal performance. To achieve better performance, it is better to optimize both the restoration module and the localization module. Intuitively, one can optimize the restoration and localization modules simultaneously in a joint training manner. However, we found this strategy did not work well. The reason is that the restoration module is in a relatively poor state in the early stage of training, and the localization module would be misled by the poor restored images produced in the early stage, finally resulting in poor localization performance. To verify our analysis, we plotted the training restoration and localization losses in Fig. 4. As shown in this figure, when the two modules are jointly optimized, the localization loss decreases slowly and takes more iterations to converge. This is due to the fact that the restoration loss is relatively large in the early stage, and the poor restored images make the localization module learn undesirable feature representations.

To better optimize the two modules in ReLoc, we should make both of them in a relatively good state. Therefore, we alternately optimize the restoration module and the localization module, the optimization algorithm is shown in Algorithm 1. Specifically, we optimize either the restoration module or the localization module in one epoch. At the first, we start to optimize the restoration module. We firstly use the discriminator to classify the plain images and the restored images, and optimize the discriminator based on  $\mathcal{L}_D$ . Then, we optimize the restoration module with the guidance of  $\mathcal{L}_R$ . After training the discriminator and the restoration module with the whole dataset, we start another epoch and only optimize the localization module with  $\mathcal{L}_L$ . The above process is repeated until the whole model becomes convergent. As shown in Fig. 4, compared to joint training, the localization loss in alternate training decreases faster and converges earlier.

TABLE I  
LOCALIZATION PERFORMANCE OF DIFFERENT RESTORATION LOSSES.

	F1	IOU	AUC
$\mathcal{L}_{MAE}$	0.515	0.396	0.940
$\mathcal{L}_{MAE} + \mathcal{L}_G$	0.523	0.404	0.944
$\mathcal{L}_{MAE} + \mathcal{L}_L$	0.542	0.419	<b>0.958</b>
$\mathcal{L}_{MAE} + \mathcal{L}_G + \mathcal{L}_L$	<b>0.567</b>	<b>0.444</b>	0.955

According to our experiments, by optimizing the restoration and localization modules in such an alternate way, the training process of ReLoc is more stable, and the model can achieve better localization performance and robustness (please refer to Table II).

#### IV. EXPERIMENTS

In this section, we evaluate the effectiveness of the proposed method. As JPEG compression is one of the most commonly used post-processing operations, we consider it as a typical example of post-processing and investigate the robustness of tampering localization against JPEG compression.

##### A. Experimental Setup

1) *Datasets*: Three tampering datasets are used for performance evaluations.

- *Certificate PS dataset*. This dataset is generated from 4,840 original certificate images that were captured by 77 different mobile phones. There are five commonly used tampering operations for certificate images, *i.e.*, splicing, copy-move, removal, text addition, and text replacement. We invited 25 experts to choose one of the five operations to tamper with every original image. The resulting tampered images are saved in uncompressed PNG format.
- *DEFACTO dataset* [47]. The tampered images in this dataset are created from the MS-COCO dataset [53] in an automatic way. Various common tampering operations are used to generate the tampered images, including copy-move, splicing, and removal. In our experiments, we randomly selected 98,000 tampered images from this dataset.
- *IMD2020 dataset* [48]. This dataset consists of 35,000 original images and 70,000 tampered images generated by GAN and inpainting methods. In addition, it also contains 2,010 tampered images collected from real scenes. We used the 2,010 realistic tampered images in our experiments.

All the aforementioned tampered images are regarded as plain images in the experiments, and we applied JPEG compression to them to obtain the distorted images. For each dataset, we randomly selected 75% images for training and used the left 25% for testing.

2) *Backbone networks*: We used SwinConv-Unet<sup>2</sup> [37] as our restoration module, which has achieved good image

<sup>2</sup><https://github.com/csxn/SCUNet>

TABLE II  
LOCALIZATION PERFORMANCE OF DIFFERENT OPTIMIZATION STRATEGIES.

	F1	IOU	AUC
Joint training	0.499	0.373	0.938
Alternate training	<b>0.567</b>	<b>0.444</b>	<b>0.955</b>

restoration performance via combining swin transformer and convolutional block. As for the localization module, we implemented it with three state-of-the-art tampering localization methods, including DFCN<sup>3</sup> [16], MVSS-net<sup>4</sup> [43], and SCSE-Unet<sup>5</sup> [10], so as to verify that ReLoc can universally improve the robustness against post-processing.

3) *Performance metrics*: As image tampering localization is a pixel-level binary classification task, we use some commonly used metrics for binary classification to evaluate the performance of the proposed framework, including F1-score, IOU (Intersection over Union), and AUC (Area Under the ROC Curve). For computing the F1-score and IOU, we applied thresholding to the predictions of all images with a fix threshold of 0.5.

4) *Implementation details and evaluation protocol*: We implemented the proposed method with PyTorch 1.9.0 and ran all the experiments with an NVIDIA V100 GPU<sup>6</sup>. In the training phase, we used 128×128 image blocks for training. Due to the limitation of GPU memory, we set the batch size as large as possible for different localization networks, namely, 56 for DFCN, 40 for SCSE-Unet, and 48 for MVSS-net. The restoration and localization modules were optimized with Adam optimizer with the default setting in PyTorch. The initial learning rate was set to 10<sup>-4</sup> for both the restoration and localization modules. When the validation loss did not descend in two consecutive epochs, we decreased the learning rate by a factor of 0.8. For the Certificate PS dataset,  $\lambda_1$ ,  $\lambda_2$ ,  $\lambda_3$ , and  $\lambda_4$  were set to 0.2, 100, 1, and 0.05, respectively, while for DEFACTO and IMD2020 datasets,  $\lambda_1$ ,  $\lambda_2$ ,  $\lambda_3$ , and  $\lambda_4$  were set to 0.2, 100, 1, and 0.1, respectively. During the testing phase, some high-resolution images could not be tested directly due to memory limitation. Hence, we used the sliding window strategy in all experiments. The window size was 512×512 and the sliding step was 512. We combined the testing results of all image blocks within an image to compute the performance metrics.

##### B. Ablation Study

In this subsection, we evaluate the effectiveness of the design of ReLoc through ablation experiments. Two key factors that would affect the performance of ReLoc has been investigated, *i.e.*, the restoration loss and optimization strategy for training the two modules. Note that the experiments were conducted on the Certificate PS dataset by using DFCN as the localization module.

<sup>3</sup><https://github.com/ZhuangPeiyu/Dense-FCN-for-tampering-localization>

<sup>4</sup><https://github.com/dong03/MVSS-Net>

<sup>5</sup><https://github.com/HighwayWu/Tianchi-FFT2>

<sup>6</sup>Code available at: <https://github.com/ZhuangPeiyu/ReLoc>

TABLE III

LOCALIZATION PERFORMANCE FOR THREE DATASETS IN DIFFERENT TRAINING/TESTING SITUATIONS. THE FIRST SITUATION (GRAY BACKGROUND) SHOWS THE RESULTS FOR PLAIN IMAGES AND CAN BE REGARDED AS THE PERFORMANCE UPPER BOUND OF EACH METHOD. THE REST SITUATIONS SHOW THE RESULTS FOR DISTORTED IMAGES, WHERE THE BEST RESULTS ARE IN BOLD.

Localization methods	Situations	Certificate PS			DEFACTO			IMD2020		
		F1	IOU	AUC	F1	IOU	AUC	F1	IOU	AUC
DFCN	$\mathcal{M}^P\{\mathbf{I}^P\}$	0.912	0.858	0.993	0.556	0.484	0.950	0.352	0.245	0.859
	$\mathcal{M}^P\{\mathbf{I}^D\}$	0.062	0.034	0.626	0.026	0.019	0.715	0.259	0.171	0.808
	$\mathcal{M}^{D P}\{\mathbf{I}^D\}$	0.484	0.369	0.905	0.404	0.338	0.880	0.281	0.182	0.834
	$\mathcal{M}^{ReLoc}\{\mathbf{I}^D\}$	<b>0.567</b>	<b>0.444</b>	<b>0.955</b>	<b>0.429</b>	<b>0.359</b>	<b>0.888</b>	<b>0.329</b>	<b>0.223</b>	<b>0.849</b>
SCSE-Unet	$\mathcal{M}^P\{\mathbf{I}^P\}$	0.925	0.878	0.996	0.706	0.635	0.978	0.501	0.389	0.921
	$\mathcal{M}^P\{\mathbf{I}^D\}$	0.031	0.019	0.587	0.281	0.238	0.896	0.391	0.296	0.879
	$\mathcal{M}^{D P}\{\mathbf{I}^D\}$	0.604	0.484	0.949	0.582	0.516	0.949	0.416	0.306	0.898
	$\mathcal{M}^{ReLoc}\{\mathbf{I}^D\}$	<b>0.651</b>	<b>0.538</b>	<b>0.962</b>	<b>0.611</b>	<b>0.543</b>	<b>0.953</b>	<b>0.454</b>	<b>0.340</b>	<b>0.915</b>
MVSS-net	$\mathcal{M}^P\{\mathbf{I}^P\}$	0.789	0.687	0.993	0.558	0.478	0.943	0.384	0.280	0.838
	$\mathcal{M}^P\{\mathbf{I}^D\}$	0.011	0.006	0.642	0.161	0.126	0.849	0.228	0.161	0.756
	$\mathcal{M}^{D P}\{\mathbf{I}^D\}$	0.391	0.270	0.916	0.507	0.429	0.910	0.314	0.216	<b>0.819</b>
	$\mathcal{M}^{ReLoc}\{\mathbf{I}^D\}$	<b>0.410</b>	<b>0.288</b>	<b>0.942</b>	<b>0.515</b>	<b>0.438</b>	<b>0.917</b>	<b>0.323</b>	<b>0.228</b>	0.810

1) *Restoration loss*: To investigate the impact of different restoration losses on the performance of ReLoc, we used different losses and their combinations to optimize the restoration module. The experimental results are shown in Table I. We can observe that compared with using only  $\mathcal{L}_{MAE}$ , adding  $\mathcal{L}_G$  is effective to help the restoration module to produce better restored images. The F1-score is improved from 0.515 to 0.523. On the other hand, introducing  $\mathcal{L}_L$  to optimize the restoration module is also beneficial for improving the performance. The F1-score is increased from 0.515 to 0.542 in this case. This implies that by introducing the localization loss, the restoration module can be guided to pay more attention to strengthening the differences between the original pixels and the tampered pixels. In such a way, the distorted tampering traces can be re-enhanced. Finally, by combining  $\mathcal{L}_{MAE}$ ,  $\mathcal{L}_G$ , and  $\mathcal{L}_L$  together, the restoration module can work better, and the F1-score is improved from 0.542 to 0.567.

2) *Optimization strategy*: To evaluate which strategy is better for optimizing the two modules in ReLoc, we separately conducted experiments to train the two modules jointly and alternately. It can be seen from Table II that by alternately training the restoration and localization modules, the obtained performance is better than training them jointly. The net increases of F1-score, IOU, and AUC are 0.068, 0.071, and 0.017, respectively.

### C. Robustness against Fixed JPEG Compression

For a given JPEG image, its compression quality factor (or quantization table) is available in the JPEG file. To perform tampering localization, ideally we can build a matched detection model by collecting training images with the same quality

factor. Therefore, in this subsection we evaluate the robustness of the proposed framework against a fixed JPEG compression, where the JPEG quality factor (QF) is set to 75. We separately used DFCN, SCSE-Unet, and MVSS-net as the localization module in ReLoc, and conducted experiments in four different training/testing situations. The result are shown in Table III. From this table, we mainly obtain two observations.

Firstly, when a model trained with plain images is used to test distorted images (*i.e.*, the case  $\mathcal{M}^P\{\mathbf{I}^D\}$ ), the localization performance would be significantly degraded. This is not surprising as the tampering traces are weak in distorted images. The performance decline for the Certificate PS dataset is the worst, where the F1-scores are decreased close to 0. The reason is that the plain tampered images in this dataset are uncompressed, and there are considerable differences between the tampered and original regions. The localization model can easily learn discriminative features from the plain images, but the learned features are not suitable for resisting JPEG compression. In the DEFACTO and IMD2020 datasets, some plain tampered images have been undergone JPEG compression after tampering, so the models  $\mathcal{M}^P$  trained with these datasets could somewhat adapt to JPEG compression and thus perform relatively better.

More importantly, we observe that using distorted tampered images to directly train the localization network can improve the robustness against JPEG compression to a certain extent, but the improvement is not as significant as the use of ReLoc. For example, by using DFCN as the localization module, the average improvement of F1-score between  $\mathcal{M}^{D|P}\{\mathbf{I}^D\}$  and  $\mathcal{M}^P\{\mathbf{I}^D\}$  is 0.274, while the average improvement is 0.326 when using ReLoc. Similar results can be obtain by considering SCSE-Unet and MVSS-net. On average, the improvements



TABLE IV  
THE LOCALIZATION PERFORMANCE REGARDING TO DIFFERENT JPEG COMPRESSIONS.

Dataset	Localization methods	Sistuations	QF60			QF70			QF80		
			F1	IOU	AUC	F1	IOU	AUC	F1	IOU	AUC
Certificate PS	DFCN	$\mathcal{M}^{D P}\{\mathbf{I}^D\}$	0.443	0.335	0.880	0.466	0.357	0.891	0.494	0.381	0.903
		$\mathcal{M}^{ReLoc}\{\mathbf{I}^D\}$	<b>0.479</b>	<b>0.370</b>	<b>0.900</b>	<b>0.513</b>	<b>0.396</b>	<b>0.938</b>	<b>0.584</b>	<b>0.470</b>	<b>0.957</b>
	SCSE-Unet	$\mathcal{M}^{D P}\{\mathbf{I}^D\}$	0.509	0.391	0.928	0.531	0.407	0.939	0.578	0.453	0.951
		$\mathcal{M}^{ReLoc}\{\mathbf{I}^D\}$	<b>0.510</b>	<b>0.391</b>	<b>0.930</b>	<b>0.609</b>	<b>0.486</b>	<b>0.955</b>	<b>0.700</b>	<b>0.589</b>	<b>0.969</b>
	MVSS-net	$\mathcal{M}^{D P}\{\mathbf{I}^D\}$	0.328	0.216	0.874	0.337	0.222	0.886	0.348	0.231	0.899
		$\mathcal{M}^{ReLoc}\{\mathbf{I}^D\}$	<b>0.337</b>	<b>0.222</b>	<b>0.893</b>	<b>0.374</b>	<b>0.254</b>	<b>0.920</b>	<b>0.441</b>	<b>0.316</b>	<b>0.938</b>
DEFACTO	DFCN	$\mathcal{M}^{D P}\{\mathbf{I}^D\}$	0.402	0.338	0.889	0.409	0.345	0.890	0.463	0.398	0.907
		$\mathcal{M}^{ReLoc}\{\mathbf{I}^D\}$	<b>0.421</b>	<b>0.354</b>	<b>0.896</b>	<b>0.432</b>	<b>0.365</b>	<b>0.896</b>	<b>0.485</b>	<b>0.415</b>	<b>0.910</b>
	SCSE-Unet	$\mathcal{M}^{D P}\{\mathbf{I}^D\}$	0.588	0.518	<b>0.951</b>	0.594	0.525	<b>0.953</b>	0.629	0.562	<b>0.959</b>
		$\mathcal{M}^{ReLoc}\{\mathbf{I}^D\}$	<b>0.600</b>	<b>0.533</b>	0.950	<b>0.604</b>	<b>0.538</b>	0.952	<b>0.634</b>	<b>0.567</b>	0.958
	MVSS-net	$\mathcal{M}^{D P}\{\mathbf{I}^D\}$	0.461	0.392	<b>0.914</b>	0.467	0.398	<b>0.916</b>	0.507	0.432	0.900
		$\mathcal{M}^{ReLoc}\{\mathbf{I}^D\}$	<b>0.477</b>	<b>0.404</b>	0.910	<b>0.489</b>	<b>0.415</b>	0.911	<b>0.532</b>	<b>0.455</b>	<b>0.925</b>
IMD2020	DFCN	$\mathcal{M}^{D P}\{\mathbf{I}^D\}$	0.287	0.186	0.829	0.289	0.188	0.835	0.290	0.189	0.836
		$\mathcal{M}^{ReLoc}\{\mathbf{I}^D\}$	<b>0.338</b>	<b>0.229</b>	<b>0.841</b>	<b>0.344</b>	<b>0.233</b>	<b>0.854</b>	<b>0.357</b>	<b>0.244</b>	<b>0.861</b>
	SCSE-Unet	$\mathcal{M}^{D P}\{\mathbf{I}^D\}$	0.429	0.320	<b>0.897</b>	0.429	0.321	0.900	0.436	<b>0.356</b>	0.903
		$\mathcal{M}^{ReLoc}\{\mathbf{I}^D\}$	<b>0.446</b>	<b>0.334</b>	<b>0.897</b>	<b>0.454</b>	<b>0.340</b>	<b>0.901</b>	<b>0.459</b>	0.347	<b>0.905</b>
	MVSS-net	$\mathcal{M}^{D P}\{\mathbf{I}^D\}$	0.320	0.224	<b>0.813</b>	0.331	<b>0.234</b>	<b>0.814</b>	0.323	<b>0.231</b>	<b>0.813</b>
		$\mathcal{M}^{ReLoc}\{\mathbf{I}^D\}$	<b>0.331</b>	<b>0.230</b>	0.812	<b>0.334</b>	0.233	<b>0.814</b>	<b>0.325</b>	0.228	0.812

of F1-score between the cases  $\mathcal{M}^{ReLoc}\{\mathbf{I}^D\}$  and  $\mathcal{M}^{D|P}\{\mathbf{I}^D\}$  are 0.052, 0.038, and 0.012, respectively for DFCN, SCSE-Unet, and MVSS-net. Based on these experimental results, it can be concluded that the proposed framework can indeed effectively improve the robustness of tampering localization against fixed JPEG compression.

#### D. Robustness against Multiple JPEG Compressions

As we all know, in real-world scenarios, different tampered images are usually subjected to different JPEG compressions. Training a specific ReLoc model for each JPEG compression under investigation is impractical because it would be time-consuming and the implementations of JPEG compression would vary from manufacturers and software. Therefore, in this subsection, we evaluate the robustness against different JPEG compressions by using a single model.

To generate distorted images for model training, we sampled uniformly the JPEG QFs between 70 and 100, similar to what was done in [10]. In the testing phase, three different QFs were considered, *i.e.*, 60, 70, and 80. Two training/testing situations,  $\mathcal{M}^{D|P}\{\mathbf{I}^D\}$  and  $\mathcal{M}^{ReLoc}\{\mathbf{I}^D\}$ , were involved in this experiment. The experimental results are shown in Table IV. From this table, we observe that no matter which localization method was adopted, the localization performance of  $\mathcal{M}^{ReLoc}\{\mathbf{I}^D\}$  is better than that of  $\mathcal{M}^{D|P}\{\mathbf{I}^D\}$ . When the

testing QF is 80, the improvements of F1-score averaged over three datasets are 0.060, 0.050, and 0.040 for DFCN, SCSE-Unet, and MVSS-net, respectively. The average improvements for QF 70 are relatively slighter, which are 0.042, 0.037, and 0.021 for DFCN, SCSE-Unet, and MVSS-net, respectively. When the testing QF is unseen in the training phase (*i.e.*, QF 60), the average improvements achieved by ReLoc for DFCN, SCSE-Unet, and MVSS-net are 0.035, 0.010, and 0.012, respectively, which are still considerable. These experimental results indicate that ReLoc is also effective for improving the robustness against multiple JPEG compressions.

#### E. Qualitative Comparisons

In order to assess the performance intuitively, we show some examples of tampering localization results in Fig. 5. In each example in this figure, from top to bottom,  $\mathbf{I}^D$  was generated through compressing  $\mathbf{I}^P$  with QFs 60, 70, and 80, respectively. By comparing the results of  $\mathcal{M}^P\{\mathbf{I}^P\}$  and  $\mathcal{M}^P\{\mathbf{I}^D\}$ , we can see that the latter case would lead to much more false alarms and/or missed detections. Although this phenomenon can be mitigated via fine-tuning the localization network with distorted images (*i.e.*,  $\mathcal{M}^{D|P}\{\mathbf{I}^D\}$ ), there are still more false predictions compared to the proposed method (*i.e.*,  $\mathcal{M}^{ReLoc}\{\mathbf{I}^D\}$ ). For instance, the tampered region in the fourth example is the tennis ball. The localization result is

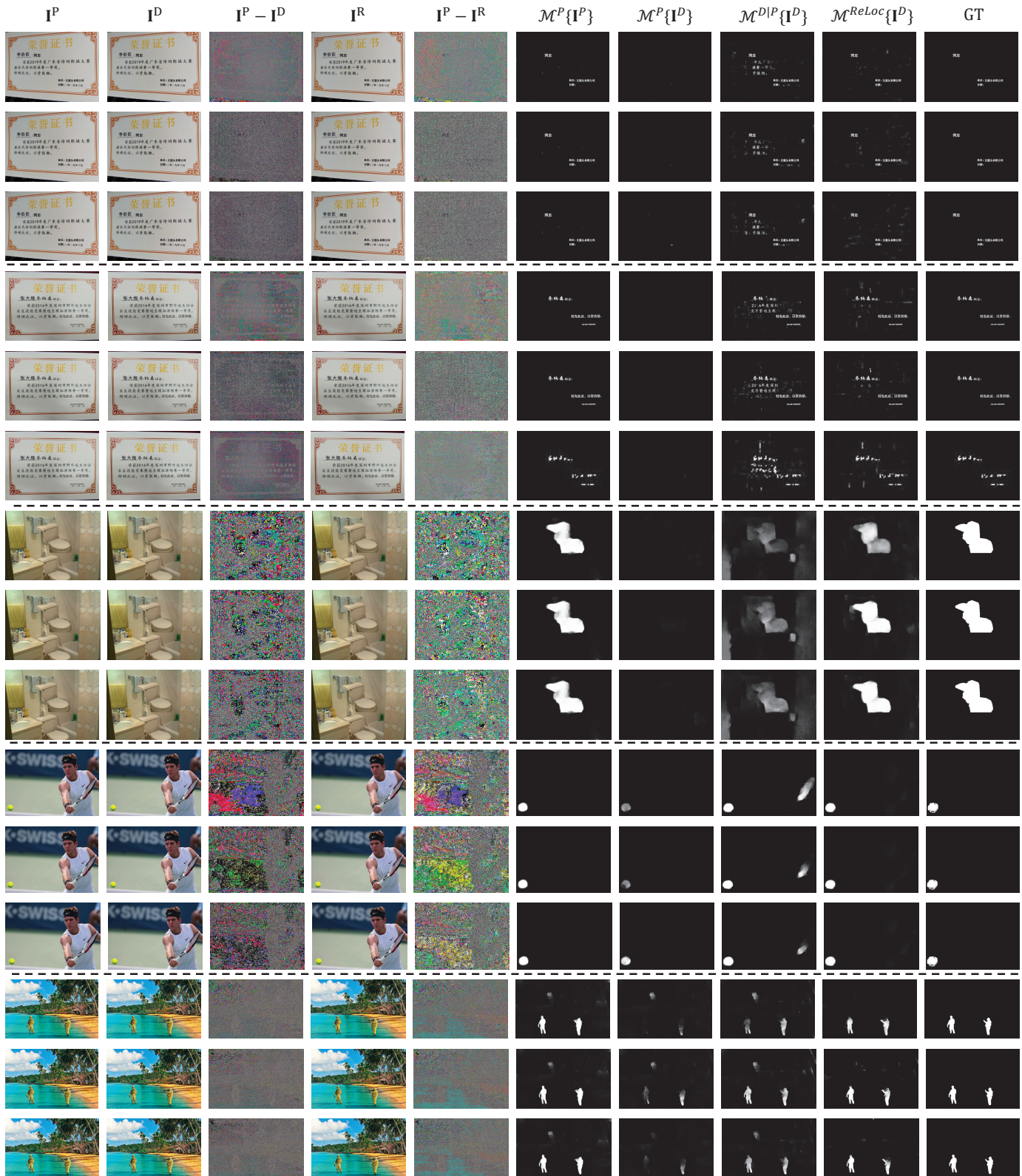


Fig. 5. Examples of tampering localization results in different situations. Each super-row (separated by dashed lines) corresponds to an example. In each example, the distorted images  $I^D$  from top to bottom were compressed with JPEG quality factors 60, 70, and 80, respectively. Examples #1 and #2 are from the Certificate PS dataset, examples #3 and #4 are from the DEFACTO dataset, while the last example is from the IMD2020 dataset.

TABLE V

THE LOCALIZATION RESULTS OBTAINED BY ReLoC VIA REPLACING THE LOCALIZATION MODULE ( $\mathcal{M}_L^{ReLoc}$ ) IN A WELL-TRAINED ReLoC MODEL WITH ANOTHER LOCALIZATION MODULE TRAINED WITH PLAIN IMAGES ( $\mathcal{M}^P$ ). THE COLUMNS  $\mathcal{M}_L^{ReLoc}$  AND  $\mathcal{M}^P$  DENOTE THE TYPES OF NETWORK STRUCTURES. THE VALUES IN PARENTHESES ARE THE IMPROVEMENTS COMPARED TO THE CASE  $\mathcal{M}^P\{\mathbf{I}^D\}$ .

Dataset	$\mathcal{M}_L^{ReLoc}$	$\mathcal{M}^P$	F1	IOU	AUC
Certificate PS	DFCN	SCSE-Unet	0.441 (+0.410)	0.349 (+0.330)	0.844 (+0.257)
	SCSE-Unet	DFCN	0.404 (+0.342)	0.309 (+0.275)	0.891 (+0.265)
DEFACTO	DFCN	SCSE-Unet	0.612 (+0.331)	0.543 (+0.305)	0.953 (+0.057)
	SCSE-Unet	DFCN	0.293 (+0.267)	0.248 (+0.229)	0.859 (+0.144)

correct in the  $\mathcal{M}^P\{\mathbf{I}^P\}$  situation. However, there are missed detections in the  $\mathcal{M}^P\{\mathbf{I}^D\}$  situation, especially when the QF is low. In the  $\mathcal{M}^{D|P}\{\mathbf{I}^D\}$  situation, missed detections are decreased, but false alarms are introduced. By contrast, in the  $\mathcal{M}^{ReLoc}\{\mathbf{I}^D\}$  situation, via employing the ReLoC framework, we can accurately locate the tampered region for different QFs.

#### F. Transferability of the Restoration Module

In this subsection, we evaluate the transferability of restoration module of a well-trained ReLoC model. We firstly trained the restoration module together with a localization module using the proposed method. Then, we deployed the trained restoration module with another localization model trained with plain tampered images ( $\mathcal{M}^P$ ). We aim to evaluate whether the performance of another localization model would be improved or not by feeding it the images output by the restoration module.

As shown in Table V, compared to the results in the case  $\mathcal{M}^P\{\mathbf{I}^D\}$  (see Table III), when directly combining the restoration module trained along with DFCN and the SCSE-Unet localization model, the F1-score of SCSE-Unet is improved from 0.031 to 0.441 on the Certificate PS dataset and improved from 0.281 to 0.612 on the DEFACTO dataset. The same phenomenon can be observed when the restoration module trained along with SCSE-Unet was deployed with the DFCN. the improvements of F1-score are 0.342 and 0.267 on the Certificate PS dataset and the DEFACTO dataset, respectively. Such experimental results have verify that the restoration module in ReLoC is transferable.

#### V. CONCLUSION

In this paper, in order to improve the robustness of tampering localization against post-processing, we propose a restoration-assisted framework named ReLoC. The ReLoC framework is composed of an image restoration module and a tampering localization module. We utilize the image restoration module to recover tampering traces from distorted images. By optimizing the restoration module with pixel-level, image-level, and forensics-oriented losses, it is able to produce a restored image that is closer to the plain image, which can

help the localization module learn more discriminative and robust features. By adopting an alternate training strategy, we make the training process more stable and further improve the localization performance. Via considering JPEG compression as a typical example of post-processing, we have conducted extensive experiments to evaluate the effectiveness of ReLoC. The experimental results show that ReLoC can significantly improve the robustness of tampering localization. Moreover, our experiments show that the trained restoration module is transferable, meaning that it can be individually and flexibly deployed with other tampered localization methods.

In the future, we will further study to employ ReLoC for improving the robustness against other post-processing operations. For example, blurring, scaling, noise corruption, *etc.* On the other hand, the restoration module and the localization module in ReLoC are flexible, we will update the modules with newly proposed and more effective restoration/localization methods to further improve the robustness against various post-processing operations.

#### REFERENCES

- [1] L. Verdoliva, "Media forensics and deepfakes: An overview," *IEEE Journal of Selected Topics in Signal Processing*, vol. 14, no. 5, pp. 910–932, 2020.
- [2] I. Castillo Camacho and K. Wang, "A comprehensive review of deep-learning-based methods for image forensics," *Journal of Imaging*, vol. 7, no. 4, p. 69, 2021.
- [3] O. Mayer and M. C. Stamm, "Accurate and efficient image forgery detection using lateral chromatic aberration," *IEEE Transactions on Information Forensics and Security*, vol. 13, pp. 1762–1777, 2018.
- [4] A. C. Gallagher and T. Chen, "Image authentication by detecting traces of demosaicing," in *Proceedings of the IEEE/CVF Conference on Computer Vision and Pattern Recognition Workshops*, 2008, pp. 1–8.
- [5] H.-D. Yuan, "Blind forensics of median filtering in digital images," *IEEE Transactions on Information Forensics and Security*, vol. 6, pp. 1335–1345, 2011.
- [6] R. Salloum, Y. Ren, and C. C. Jay Kuo, "Image splicing localization using a multi-task fully convolutional network (MFCN)," *Journal of Visual Communication and Image Representation*, vol. 51, pp. 201–209, 2018.
- [7] Y. Sun, R. Ni, and Y. Zhao, "ET: Edge-enhanced transformer for image splicing detection," *IEEE Signal Processing Letters*, vol. 29, pp. 1232–1236, 2022.
- [8] J. L. Zhong and C. M. Pun, "An end-to-end Dense-InceptionNet for image copy-move forgery detection," *IEEE Transactions on Information Forensics and Security*, vol. 15, pp. 2134–2146, 2020.
- [9] D. Cozzolino, G. Poggi, and L. Verdoliva, "Efficient dense-field copy-move forgery detection," *IEEE Transactions on Information Forensics and Security*, vol. 10, no. 11, pp. 2284–2297, 2015.
- [10] H. Wu, J. Zhou, J. Tian, J. Liu, and Y. Qiao, "Robust image forgery detection against transmission over online social networks," *IEEE Transactions on Information Forensics and Security*, vol. 17, pp. 443–456, 2022.
- [11] H. Li and J. Huang, "Localization of deep inpainting using high-pass fully convolutional network," in *Proceedings of the IEEE/CVF International Conference on Computer Vision*, 2019, pp. 8301–8310.
- [12] H. Wu and J. Zhou, "IID-Net: Image inpainting detection network via neural architecture search and attention," *IEEE Transactions on Circuits and Systems for Video Technology*, vol. 32, no. 3, pp. 1172–1185, 2022.
- [13] X. Hu, Z. Zhang, Z. Jiang, S. Chaudhuri, Z. Yang, and R. Nevatia, "SPAN: Spatial pyramid attention network for image manipulation localization," in *Proceedings of the European Conference on Computer Vision*, 2020, pp. 312–328.
- [14] Y. Wu, W. AbdAlmageed, and P. Natarajan, "ManTra-Net: Manipulation tracing network for detection and localization of image forgeries with anomalous features," in *Proceedings of the IEEE/CVF Conference on Computer Vision and Pattern Recognition*, 2019, pp. 9543–9552.

- [15] X. Liu, Y. Liu, J. Chen, and X. Liu, "PSCC-Net: Progressive spatio-channel correlation network for image manipulation detection and localization," *IEEE Transactions on Circuits and Systems for Video Technology*, 2022.
- [16] P. Zhuang, H. Li, S. Tan, B. Li, and J. Huang, "Image tampering localization using a dense fully convolutional network," *IEEE Transactions on Information Forensics and Security*, vol. 16, pp. 2986–2999, 2021.
- [17] J. Hao, Z. Zhang, S. Yang, D. Xie, and S. Pu, "TransForensics: Image forgery localization with dense self-attention," in *Proceedings of the IEEE/CVF International Conference on Computer Vision*, 2021, pp. 15 055–15 064.
- [18] J. Wang, Z. Wu, J. Chen, X. Han, A. Shrivastava, S.-N. Lim, and Y.-G. Jiang, "ObjectFormer for image manipulation detection and localization," in *Proceedings of the IEEE/CVF Conference on Computer Vision and Pattern Recognition*, 2022, pp. 2364–2373.
- [19] J. Long, E. Shelhamer, and T. Darrell, "Fully convolutional networks for semantic segmentation," in *Proceedings of the IEEE/CVF Conference on Computer Vision and Pattern Recognition*, 2015, pp. 3431–3440.
- [20] O. Ronneberger, P. Fischer, and T. Brox, "U-Net: Convolutional networks for biomedical image segmentation," in *Proceedings of the International Conference on Medical Image Computing and Computer-Assisted Intervention*, 2015, pp. 234–241.
- [21] S. Ren, K. He, R. Girshick, and J. Sun, "Faster R-CNN: Towards real-time object detection with region proposal networks," *Advances in Neural Information Processing Systems*, vol. 28, 2015.
- [22] K. He, G. Gkioxari, P. Dollár, and R. Girshick, "Mask R-CNN," in *Proceedings of the IEEE/CVF International Conference on Computer Vision*, 2017, pp. 2961–2969.
- [23] A. Dosovitskiy, L. Beyer, A. Kolesnikov, D. Weissenborn, X. Zhai, T. Unterthiner, M. Dehghani, M. Minderer, G. Heigold, S. Gelly *et al.*, "An image is worth 16x16 words: Transformers for image recognition at scale," in *International Conference on Learning Representations*, 2020.
- [24] J. Fridrich and J. Kodovsky, "Rich models for steganalysis of digital images," *IEEE Transactions on Information Forensics and Security*, vol. 7, no. 3, pp. 868–882, 2012.
- [25] B. Bayar and M. C. Stamm, "Constrained convolutional neural networks: A new approach towards general purpose image manipulation detection," *IEEE Transactions on Information Forensics and Security*, vol. 13, no. 11, pp. 2691–2706, 2018.
- [26] Y. Rao and J. Ni, "Self-supervised domain adaptation for forgery localization of JPEG compressed images," in *Proceedings of the IEEE/CVF International Conference on Computer Vision*, 2021, pp. 15 034–15 043.
- [27] G. Chantas, N. P. Galatsanos, R. Molina, and A. K. Katsaggelos, "Variational Bayesian image restoration with a product of spatially weighted total variation image priors," *IEEE Transactions on Image Processing*, vol. 19, no. 2, pp. 351–362, 2010.
- [28] G. Chantas, N. Galatsanos, and A. Likas, "Bayesian restoration using a new nonstationary edge-preserving image prior," *IEEE Transactions on Image Processing*, vol. 15, no. 10, pp. 2987–2997, 2006.
- [29] R. Molina, J. Nunez, F. Cortijo, and J. Mateos, "Image restoration in astronomy: A Bayesian perspective," *IEEE Signal Processing Magazine*, vol. 18, no. 2, pp. 11–29, 2001.
- [30] A. Krizhevsky, I. Sutskever, and G. E. Hinton, "Imagenet classification with deep convolutional neural networks," *Advances in Neural Information Processing Systems*, vol. 25, 2012.
- [31] A. Vaswani, N. Shazeer, N. Parmar, J. Uszkoreit, L. Jones, A. N. Gomez, . Kaiser, and I. Polosukhin, "Attention is all you need," in *Advances in Neural Information Processing Systems*, vol. 30, 2017.
- [32] C. Dong, C. C. Loy, K. He, and X. Tang, "Learning a deep convolutional network for image super-resolution," in *Proceedings of the European Conference on Computer Vision*, 2014, pp. 184–199.
- [33] C. Dong, Y. Deng, C. C. Loy, and X. Tang, "Compression artifacts reduction by a deep convolutional network," in *Proceedings of the IEEE/CVF International Conference on Computer Vision*, 2015, pp. 576–584.
- [34] J. Kim, J. K. Lee, and K. M. Lee, "Accurate image super-resolution using very deep convolutional networks," in *Proceedings of the IEEE/CVF Conference on Computer Vision and Pattern Recognition*, 2016, pp. 1646–1654.
- [35] Y. Zhang, Y. Tian, Y. Kong, B. Zhong, and Y. Fu, "Residual dense network for image restoration," *IEEE Transactions on Pattern Analysis and Machine Intelligence*, vol. 43, no. 7, pp. 2480–2495, 2021.
- [36] Z. Wang, X. Cun, J. Bao, and J. Liu, "UFormer: A general u-shaped transformer for image restoration," *arXiv:2106.03106*, 2021.
- [37] K. Zhang, Y. Li, J. Liang, J. Cao, Y. Zhang, H. Tang, R. Timofte, and L. Van Gool, "Practical blind denoising via Swin-Conv-UNet and data synthesis," *arXiv:2203.13278*, 2022.
- [38] J. Johnson, A. Alahi, and L. Fei-Fei, "Perceptual losses for real-time style transfer and super-resolution," in *Proceedings of the European Conference on Computer Vision*, 2016, pp. 694–711.
- [39] M. Haris, G. Shakhnarovich, and N. Ukita, "Task-driven super resolution: Object detection in low-resolution images," *Communications in Computer and Information Science*, 2021.
- [40] X. Niu, B. Yan, W. Tan, and J. Wang, "Effective image restoration for semantic segmentation," *Neurocomputing*, vol. 374, pp. 100–108, 2020.
- [41] Y. Wu, W. Abd-Almageed, and P. Natarajan, "BusterNet: Detecting copy-move image forgery with source/target localization," in *Proceedings of the European Conference on Computer Vision*, 2018, pp. 168–184.
- [42] X. Wang, R. Girshick, A. Gupta, and K. He, "Non-local neural networks," in *Proceedings of the IEEE/CVF Conference on Computer Vision and Pattern Recognition*, 2018, pp. 7794–7803.
- [43] X. Chen, C. Dong, J. Ji, J. Cao, and X. Li, "Image manipulation detection by multi-view multi-scale supervision," in *Proceedings of the IEEE/CVF International Conference on Computer Vision*, 2021, pp. 14 185–14 193.
- [44] G. Huang, Z. Liu, L. Van Der Maaten, and K. Q. Weinberger, "Densely connected convolutional networks," in *Proceedings of the IEEE/CVF Conference on Computer Vision and Pattern Recognition*, 2017, pp. 4700–4708.
- [45] M.-J. Kwon, I.-J. Yu, S.-H. Nam, and H.-K. Lee, "CAT-Net: Compression artifact tracing network for detection and localization of image splicing," in *Proceedings of the IEEE/CVF Winter Conference on Applications of Computer Vision*, 2021, pp. 375–384.
- [46] R. Abecidan, V. Itier, J. Boulanger, and P. Bas, "Unsupervised JPEG domain adaptation for practical digital image forensics," in *Proceedings of the IEEE International Workshop on Information Forensics and Security (WIFS)*. IEEE, 2021, pp. 1–6.
- [47] G. Mahfoudi, B. Tajini, F. Retraint, F. Morain-Nicolier, J. L. Dugelay, and P. Marc, "DEFACITO: Image and face manipulation dataset," in *Proceedings of the European Signal Processing Conference*, 2019, pp. 1–5.
- [48] A. Novozamsky, B. Mahdian, and S. Saic, "IMD2020: A large-scale annotated dataset tailored for detecting manipulated images," in *Proceedings of the IEEE/CVF Winter Conference on Applications of Computer Vision Workshops*, 2020, pp. 71–80.
- [49] L. Van der Maaten and G. Hinton, "Visualizing data using T-SNE," *Journal of Machine Learning Research*, vol. 9, no. 11, 2008.
- [50] C. Xie, J. Wang, Z. Zhang, Y. Zhou, L. Xie, and A. Yuille, "Adversarial examples for semantic segmentation and object detection," in *Proceedings of the IEEE/CVF International Conference on Computer Vision*, 2017, pp. 1369–1378.
- [51] W. Tan, B. Yan, and B. Bare, "Feature super-resolution: Make machine see more clearly," in *Proceedings of the IEEE/CVF Conference on Computer Vision and Pattern Recognition*, 2018, pp. 3994–4002.
- [52] A. Radford, L. Metz, and S. Chintala, "Unsupervised representation learning with deep convolutional generative adversarial networks," *arXiv:1511.06434*, 2015.
- [53] T.-Y. Lin, M. Maire, S. Belongie, J. Hays, P. Perona, D. Ramanan, P. Dollár, and C. L. Zitnick, "Microsoft COCO: Common objects in context," in *Proceedings of the European Conference on Computer Vision*, 2014, pp. 740–755.